HHS Public Access

Author manuscript

J Orthop Res. Author manuscript; available in PMC 2016 December 01.

Published in final edited form as:

J Orthop Res. 2015 December ; 33(12): 1835–1845. doi:10.1002/jor.22975.

Assessment of Cortical and Trabecular Bone Changes in Two Models of Post-Traumatic Osteoarthritis

Hannah M Pauly[1], **Blair E Larson**[2], **Garrett A Coatney**[1,3], **Keith D. Button**[5], **Charlie E DeCamp**[4], **Ryan S Fajardo**[6], **Roger C Haut**[5,6], and **Tammy L Haut Donahue**[1,3]

[1]School of Biomedical Engineering, Colorado State University, Fort Collins, CO USA

[2]Department of Chemical and Biological Engineering, Colorado State University, Fort Collins, CO USA

[3]Department of Mechanical Engineering, Colorado State University, Fort Collins, CO USA

[4]Small Animal Clinical Sciences, College of Veterinary, Michigan State University, East Lansing, MI USA

[5]Orthopaedic Biomechanics Laboratories, College of Osteopathic Medicine, Michigan State University, East Lansing, MI USA

[6]Department of Radiology, Michigan State University, East Lansing, MI USA

Abstract

Subchondral bone is thought to play a significant role in the initiation and progression of the post-traumatic osteoarthritis. The goal of this study was to document changes in tibial and femoral subchondral bone that occur as a result of two lapine models of anterior cruciate ligament injury, a modified ACL transection model and a closed-joint traumatic compressive impact model. Twelve weeks post-injury bones were scanned via micro-computed tomography. The subchondral bone of injured limbs from both models showed decreases in bone volume and bone mineral density. Surgical transection animals showed significant bone changes primarily in the medial hemijoint of femurs and tibias, while significant changes were noted in both the medial and lateral hemijoints of both bones for traumatic impact animals. It is believed that subchondral bone changes in the medial hemijoint were likely caused by compromised soft tissue structures seen in both models. Subchondral bone changes in the lateral hemijoint of traumatic impact animals are thought to be due to transmission of the compressive impact force through the joint. The joint-wide bone changes shown in the traumatic impact model were similar to clinical findings from studies investigating the progression of osteoarthritis in humans.

Corresponding Author: Tammy L. Haut Donahue, 1374 Campus Delivery, Department of Mechanical Engineering, Colorado State University, Fort Collins, CO 80523, Tammy.Donahue@ColoState.edu, (970) 491-1319.

Author contributions: HM Pauly oversaw data collection and analysis, complied all data, and prepared the manuscript, BE Larson and GA Coatney participated in data collection and analysis, KD Button assisted in surgeries and sample collection, CE Decamp carried out all animal surgeries, RS Fajardo conducted magnetic resonance imaging and compiled results, RC Haut and TL Haut Donahue designed the study and oversaw all work. All authors reviewed and edited the manuscript. All authors have read and approved the final submitted manuscript.

Keywords

knee; subchondral bone; anterior cruciate ligament; micro-computed tomography

Introduction

Post-traumatic osteoarthritis (PTOA) is characterized by the degradation of joint structures following a traumatic injury[1]. Although PTOA can develop from a variety of accidents or injuries, it is most commonly seen after sports injuries that have resulted in anterior cruciate ligament (ACL) and meniscal tears[2]. Noncontact ACL injuries often involve a jump landing on one or both legs[3]. The excessive axial compressive loading experienced during a jump landing can generate approximately six times body weight through the knee joint in approximately 500 ms[4]. This high intensity and rate of loading in the knee can cause excessive anterior tibial translation which contributes to tearing of joint structures[5].

Although PTOA is clinically characterized by a loss of cartilage[6], subchondral bone is thought to play a significant role in the initiation and progression of the disease[7]. In healthy bone, osteoclasts and osteoblasts carry out bone resorption and formation in a balanced process that maintains bone mass, repairs damage to bones and adapts bone structure to changes in mechanical loading[8]. During OA pathogenesis the architecture of subchondral bone can be modified via bone remodeling[9]. When rates of bone resorption are high and rates of bone formation are low, bone can become hypomineralized, resulting in a lowered elastic modulus[10,11]. Conversely, during periods of low bone resorption, bones become hypermineralized, resulting in an increased elastic modulus and bone that is more brittle, increasing risk of fracture under normal loads[12]. These changes in subchondral bone mineralization may affect the overall size and shape of the subchondral bone plate, causing cartilage to be exposed to abnormal loading regimes, and thus advance the process of cartilage degradation[13,14]. Furthermore, reactivation of the tidemark[13] that stimulates remodeling of the calcified cartilage can contribute to thinning of the articular cartilage thereby accelerating osteoarthritic changes[7,15].

The chronic advancement of PTOA following an ACL tear has been previously studied with the use of a surgical ACL transection (ACLT) animal model[16–20]. Although most transection models demonstrate progressive degeneration of cartilage, they only assess changes in the joint that occur due to an isolated tear of the ACL. Clinically, meniscal damage is shown in up to 82% of human knees with traumatically ruptured ACLs[21], and osteochondral lesions occur in over 80% of ACL injury cases[22]. It has been hypothesized that the traumatic loading sustained during the acute injury induces significant bone damage that contributes to the progression of OA[9]. Despite promising results of previous traumatic injury models[23–25], they have been limited in the characterization of bone changes and results have not been compared to traditional transection models[26].

Two new models of post-traumatic osteoarthritis have been developed to better replicate the injuries documented clinically in human ACL cases. These models attempt to account for occult damages to soft tissue and bone which occur at the time of ACL injury. The first model is a modified ACL transection model (mACLT) in which the ACL undergoes a full

surgical transection and the medial and lateral menisci each undergo a partial transection[27] (Figure 1A). Although ACL transection models have previously been combined with partial or total meniscectomies[20,28], the mACLT model is the first to examine radial transections of both the medial and lateral menisci. The complex tears administered in the mACLT model are an attempt to simulate those seen often in the post-trauma clinical setting[29]. The second model is a closed-joint traumatic loading model (ACL-failure, ACLF) in which a gravity accelerated mass is dropped onto the tibiofemoral joint to cause impact-induced ruptures of the ACL and menisci[30] (Figure 1B). The ACLF model will enable an evaluation of the progression of PTOA following combined ACL and meniscal injuries that occur due to a large axial compressive load on the knee.

The goal of the current study was to assess chronic changes in subchondral cortical and trabecular bone of femurs and tibias that occur in both the ACLF and mACLT models. It was hypothesized that both models would show progressive changes in subchondral bone and that the ACLF model would result in more progressive changes, mimicking those often documented in human PTOA.

Methods

Experimental Animal Models

For this study, 12 skeletally mature Flemish Giant rabbits (5.5 ± 0.5 kg, 9–12 months of age) were used. The study was approved by the Michigan State University and Colorado State University All-University Committees on Animal Use and Care. All animals were housed in individual cages (60 × 60 × 14 inches) for the duration of the study. Half of the animals were randomly assigned to the mACLT group (4 male rabbits and 2 female rabbits) and underwent a surgical transection of the ACL and menisci, as previously described[27]. Briefly, while under anesthesia (2% isoflurane and oxygen), the right limb of each animal was opened surgically and the ACL was transected. The medial meniscus was transected radially in the white zone of the central portion of its main body, with a longitudinal cut extending in both the anterior and posterior directions. The lateral meniscus was also transected radially, but, due to space restrictions within the lateral compartment of the knee, the longitudinal cut was more minor and extended only anteriorly (Figure 1A).

The remaining six animals (5 male rabbits and 1 female rabbit) were subjected to an impact-induced rupture of the ACL and menisci (ACLF) using a closed joint injury technique, as previously described[30–32] (Figure 1B). Briefly, animals were anesthetized (2% isoflurane and oxygen) and positioned in a custom test fixture in a supine position with the right knee flexed at 90°. The right foot was fixed in a custom designed boot to maintain the flexion angle prior to impact, while the tibia was left unconstrained to allow for anterior translation of the tibia. A 1.75 kg mass was dropped onto the femur from a height of 75 cm. A pre-crushed, deformable impact surface (Hexcel, 3.76 MPa crush strength) was used to ensure uniform load distribution over the femur. MRI was used to verify ACL rupture immediately after injury and to document the condition of each joint immediately prior to euthanasia.

For all animals the left limb was used as a non-injured control. A licensed veterinary technician monitored all rabbits after injury for pain and administered buprenorphine (0.3

ml/kg BW) every 8 hours for 72 hours after surgery. The animals were sacrificed after 12 weeks. Immediately after euthanasia femurs and tibias were harvested and fixed in neutral buffered formalin.

Magnetic Resonance Imaging

Imaging was performed on a GE (Waukesha, WI) HDxt 3.0 T magnet utilizing an 8 channel HD wrist coil. Sequences included sagittal and coronal proton density, 3000–5000 ms repetition time, 32–34 ms time to echo, 62.5 kHz receiver bandwidth, 2 excitations, 1.5 mm slice thickness with 0 interslice gap, 512 × 384 matrix size, and an 8 cm field of view; as well as sagittal and coronal fat suppressed proton density, 3000–5000 ms repetition time, 32–34 ms time to echo, 50 kHz receiver bandwidth, 2 excitations, 1.5 mm slice thickness with 0 interslice gap, 416 × 256 matrix size, and an 8 cm field of view. The MRI images were assessed for evidence of intermedullary edema, intraosseous cysts, and osteophytes by a fellowship-trained musculoskeletal radiologist (RSF) with 9 years of experience.

Micro-computed Tomography (μCT)

Bones from each animal were scanned in formalin via micro-computed tomography (Scanco μCT 80, Scanco Medical AG, Brüttisellen, Switzerland) with an isotropic voxel size of 25 μm. Four spatially distributed cylindrical volumes of interest (VOI) were identified for each tibia and femur based on anatomical markers (Figure 2). VOIs were placed such that the location of measurement corresponded to locations of assessment of articular cartilage mechanical properties, as described in Fischenich et al., 2014[32]. To achieve this, prior to scanning measurements were taken from femurs and tibias to determine the location of interest in relation to the outer margins of the bone. Based on those measurements, a grid system was established similar to methods described in Batiste et al. 2004 to position the VOIs correctly within the trabecular bone[33]. Trabecular bone VOIs were located immediately under the cortical bone plate and consisted entirely of trabecular bone. Cortical bone VOIs began at the joint margin and ended at the trabecular bone and were determined using manual segmentation by a single operator (BEL). Using the built in μCT evaluation software (Scanco Medical AG IPL v4.05, Brüttisellen, Switzerland) the following measurements were obtained: volumetric trabecular material bone mineral density ($mgHA/cm^3$) (Tb.BMD), trabecular bone volume fraction (bone volume/total volume, Tb.BV/TV), trabecular number (Tb.N), trabecular thickness (mm) (Tb.Th), trabecular separation (mm) (Tb.Sp), cortical material bone mineral density ($mgHA/cm^3$) (Ct.BMD), and cortical bone porosity (Ct.Po). The volume of osteophytes (mm^3) in the injured limbs was determined by a single operator (BEL) manually outlining new bone growth on every 10^{th} consecutive μCT slice and then morphing the outlines together (Figure 2A, 2C). Osteophytic bone was identified based on its reduced bone mineral density and the growth of new bone tissue outside the margins of the normal bone.

Histology

Femurs and tibias were decalcified using 20% formic acid. Prior to paraffin embedding, tibial plateaus were sectioned coronally at the midpoint in the anterior-posterior frame of reference, while each femoral condyle was sectioned sagittally at the midpoint of the condyle. Specimens were then paraffin embedded, sectioned at 6 μm and stained using

Hematoxlyin, Safranin-O (Saf-O), and Fast Green (FG). The sections were imaged using a Nikon Eclipse E800 microscope (Nikon Inc, Melville, NY) and SPOT RTslider camera (SPOT Imaging Solutions, Sterling Heights, MI). Cortical bone thickness was determined using ImageJ (NIH, Bethesda, MD, with FIJI package). Five replicate measurements of cortical bone thickness were taken at two different locations on the medial and lateral aspects of each femur and tibia. The measurement locations were determined based on anatomical markers. The thickness of the cortical bone was defined as the mean perpendicular distance across each of the medial and lateral aspects of the femur and tibia from the transition of calcified cartilage and cortical bone to a manually delineated point of the cortical and trabecular bone interface/bone-marrow space (Figure 3).

Statistics

For the cortical and trabecular bone parameters and histology measurements, mixed model ANOVAs with Tukey post-hoc tests were performed on the data using SAS software (SAS Institute, Cary, NC, USA) to compare injured limbs to uninjured control limbs for all measured parameters. A mixed model ANOVA with Tukey post-hoc tests were used to compare ACLF animals to ACLT animals for the presence of osteophytes. Statistically significant differences were determined at $p \leq 0.05$.

Results

Experimental Animal Models

All ACLF animals suffered a ruptured ACL and meniscal tears on the injured limb. ACL injury was confirmed via palpation, and acute soft tissue injuries were documented with MRI[32]. According to observations from the veterinary technician (JA), rabbits in both the ACLF and mACLT groups favored the traumatized limb for 1–3 days after injury, but returned to normal gait thereafter. Normal gait consisted of daily movement within cage using low activity level, calm movements without significant exercise.

Magnetic Resonance Imaging

Acute MR images of the ACLF and mACLT animals showed no gross bone fractures or bruising in control or traumatized limbs. One mACLT animal presented with a small intraosseous ganglion at the femoral origin of the anterior cruciate ligament immediately after surgery, likely a result of surgical trauma. Acutely, ACLF animals most commonly had damage to both hemijoints primarily occurring in the posterior region on the menisci. The MRIs obtained 12 weeks post trauma documented chronic bone damage as well as progressive damage to both the menisci and cartilage. No control limbs showed bone damage 12 weeks after injury. Osteophyte formation was identified in MRIs of the injured limbs in three out of six mACLT animals and in five of six ACLF animals. Osteophytes in the ACLF animals were typically located dispersed throughout the patellofemoral, medial tibiofemoral, and lateral tibiofemoral knee compartments (Figure 4A), but in mACLT animals the osteophytes were primarily restricted to the medial tibiofemoral compartment (Figure 4D). Intraosseous ganglia or cysts were not identified in any of the mACLT animals 12 weeks after injury, whereas intraosseous cysts were identified in the intercondylar femur and tibia of two ACLF animals (Figure 4B). Additionally, intermedullary edema was

identified in the tibial metaphysis of one ACLF animal (Figure 4C), and in none of the mACLT animals.

Micro-Computed Tomography

Trabecular Bone—The average trabecular bone volume fraction was approximately 0.5 for all samples (Figure 5A). When compared to the uninjured control limbs, the animals from both models showed a trend for a decreased trabecular bone volume fraction in the injured limb. For the mACLT animals, significantly lower values of trabecular bone volume fraction were documented in the medial hemijoints of both the femur and tibia of injured limbs. These decreases corresponded to approximately 15% loss of trabecular bone volume in the injured limbs. In the ACLF animals there was an approximately 17% loss of bone volume in the injured limbs compared to control limbs, and that loss was significant in both hemijoints of the femur. Trabecular bone mineral density also tended to be lower in the injured limbs compared to control limbs with significant differences seen in the medial and lateral femurs as well as the medial tibia of mACLT animals, and in the lateral femur and the medial and lateral tibia of ACLF animals (Figure 5B). These significant changes corresponded to an approximately 3% loss of bone mineral density in the injured limbs.

Measures of trabecular bone morphometry showed an average of 2.5 trabecular struts per millimeter in control limbs, with each trabecular strut ~0.2 mm thick, separated by ~0.2 mm of void space (Table 1). Injured limbs had an average of 2.3 struts per millimeter, with the struts being ~0.17mm thick and separated by spaces of ~0.26 mm. The only statistically significant difference between control and injured limbs was in the lateral tibia of ACLF animals with a significant increase in trabecular separation of the injured limbs compared to control limbs.

Cortical Bone—Similar to trabecular bone, cortical bone porosity tended to be higher in the injured limbs compared to control limbs (Figure 6A). Significantly higher cortical porosity was observed in the medial tibia of both mACLT and ACLF animals. The differences corresponded to an increase of approximately 10% in cortical bone porosity for the injured limbs. Finally, significantly lower cortical bone mineral densities were noted in the medial femur of mACLT animals and the lateral femur and medial tibia of ACLF animals (Figure 6B). The lower cortical bone mineral densities corresponded to an approximately 6% loss of bone mineral density for the injured limbs. Generally speaking, larger decreases in cortical bone volume and BMD were documented in the ACLF animals versus the mACLT animals.

Osteophytes—No osteophytes were identified on control limbs, however osteophytes were present on injured limbs of both the mACLT and ACLF animals (Figure 7). There was an average osteophyte volume of approximately 75 mm^3 for injured limbs of the mACLT animals and 110 mm^3 for ACLF animals (Figure 8). There was also a significantly larger volume of osteophytes on the tibias of ACLF animals than on tibias of mACLT animals, approximately 120 mm^3 versus 60 mm^3 respectively.

Histology—The thickness of cortical bone ranged from 0.25 – 0.75 mm (Figure 9). There were no significant differences in the subchondral cortical bone thickness for either mACLT or ACLF injured limbs when compared to the control limbs. However, the subchondral cortical bone on injured limbs of ACLF animals showed a slight trend toward thickening while the subchondral cortical bone on injured limbs of mACLT animals showed a slight trend toward thinning.

Discussion

MRI, μCT and histology characterization of rabbit knee joints subjected to tears of the ACL and menisci (either though surgical transection or traumatic loading) demonstrated significant decreases in the quantity and quality of subchondral trabecular and cortical bone 12 weeks post-injury. The decrease in bone quantity was manifested by a decreased bone volume fraction and increased spacing between trabecular struts for trabecular bone, and an increase in porosity. A loss of bone mineral density indicated decreases in overall bone quality.

Even with similar trends for decreases in bone volume and bone mineral density, it was clear in this study that the progression of PTOA was significantly affected by type of model used to induce ACL and meniscal injuries (Figure 10). In mACLT animals the changes in subchondral bone observed after injury were largely restricted to the medial compartment. The absence of an intact anterior cruciate ligament may have resulted in abnormal force distribution across the joint, with additional load being transferred to the medial compartment[34,35]. In an intact knee the anterior cruciate ligament acts to prevent excessive anterior tibial translation, however when the ACL is compromised the medial meniscus likely undergoes excessive loading as it acts to restrict anterior tibial translation[36]. Recent studies have shown the areas of cartilage damage correlate directly with areas of meniscal damage[37], and the same may be true for the subchondral bone below compromised menisci. Similar to our results, other ACL transection models have documented more extensive tissue damage in the medial hemijoint compared to the lateral hemijoint[16,28,38,39]. One limitation of the use of Flemish Giant rabbits in this study is that rabbits have relatively low activity levels and do not favor excessive exercise. However if changes in bones volume and bone mineral density were due to general inactivity we have expected to equal changes in both the injured and uninjured limb over the course of the study.

Other research groups have assessed changes that occur to subchondral bone in an ACLT injury model[17–19,38,40]. Batiste et al., for example, identified a significant decrease in bone mineral density in a longitudinal lapine ACLT model 4 and 8 weeks post-surgery, with bone mineral density values returning to normal 12 weeks post-surgery[16]. This biphasic response of bone mineral density to injury, first decreasing and subsequently increasing, has been identified in several other studies. It is suggestive of an active bone remodeling process taking place post injury[41]. In contrast, a surgical transection model in canines identified a decrease in bone mineral density as early as three weeks post-surgery with subsequent decreases to 12 weeks post-surgery[18]. A meniscectomized model of PTOA development in rabbits (with no ACL injury) documented decreases in bone mineral density up to 40 weeks post-surgery[40]. An ovine meniscectomy model indicated that decreases in bone mineral

density did not occur until 6 months post-surgery, suggesting a slower progression of PTOA after injury in large animals[42]. Overall, ACLT models have demonstrated decreases in bone volume and bone mineral density very similar to the findings of the present study, however the data are highly dependent on time point.

In contrast to the mACLT model, animals that underwent a traumatic rupture of the ACL and menisci showed bone changes in both hemijoints of the injured limbs at 12 weeks. The more global injury pattern in these animals may be the result of the acute force transmitted across the joint during impact. This initial traumatic compressive force has been previously shown to cause micro-cracks near the calcified cartilage/subchondral plate in both compartments of the tibia and femur at 12 weeks[43]. Additionally, ACLF animals showed more pervasive intramedullary edema, bone cysts and osteophyte formation. Because the formation of osteophytes is thought to be triggered by alterations in joint biomechanics[44], the more prominent osteophytes on tibias and femurs of the ACLF animals (as identified by both μCT and MRI) may indicate more aggressive bone remodeling in the ACLF model post trauma due to occult microdamages induced by the acute compressive impact force across the joint. In addition to osteophytes, intermeduallary edema and cysts have been identified clinically as a consequence of acute knee injury[45] and were also identified in the ACLF animals. Previous studies have documented that the locations of intramedullary edema are closely associated with areas of severe articular cartilage loss[46]. The association of edema with cartilage damage suggests that the damaged bone may be unable to support mechanical load, which could result in the degradation of cartilage[47]. Based on these results the ACLF model appeared to replicate some of the multifactorial injuries documented in the traumatically-injured human knee.

Since PTOA is a “whole joint” disease it is important to consider changes to the subchondral bone in relation to degeneration of other joint structures. Damage to menisci and articular cartilage of mACLT and ACLF animals has been previous assessed[27,32]. Briefly, the ACLF injury model resulted in damage to the medial and lateral menisci, primarily complex tears that significantly propagated after 12 weeks. Assessments of meniscal mechanical properties and glycosaminoglycan (GAG) presence found significant decreases in instantaneous and equilibrium elastic moduli as well as decreased GAG staining intensity and coverage. Articular cartilage damage was also observed at 12 weeks, most notably significant cartilage fissures and fibrillation as well as loss of tidemark integrity which is indicative of tissue degeneration. Similar to the menisci, there was also a decrease in GAG content of the articular cartilage of injured limbs as well as diminished mechanical properties. Overall meniscal damage was present in both hemijoints of injured limbs but articular cartilage damage was more prominent in the medial hemijoint. Damage to the menisci and articular cartilage may have contributed to abnormal loading regimes within the joint which could have advanced the progression of subchondral bone damage.

Due to highly variable loading regimes, it is difficult to compare previous traumatic models with the ACLF model used in this study[23–26]. Borelli et al., impacted the medial femoral condyle cartilage in an open joint to initiate the progression of PTOA in rabbits and documented an increase in trabecular bone volume directly beneath the point of impact[23]. However, these results may be attributed to the small size (3 mm in diameter) of the

pendulum device used to impact the cartilage, since no changes in femoral trabecular bone were documented at sites distal to the point of impact. Studies using a closed-joint patellofemoral impact model have identified significant thickening of subchondral cortical bone at 12 weeks after injury[24] and at 24 and 36 weeks after injury[25], but the studies have not investigated subchondral trabecular bone. One early study investigated chronic overloading of a rabbit knee joint and documented a significant decrease in subchondral cortical bone porosity, which may be a result of remodeling in response to repetitive impulsive loads applied for long periods of time[26]. Despite these limited studies, the present study appeared to follow similar trends of bone remodeling after traumatic injury to the knee joint.

Most notably, the decreases in bone volume and bone mineral density in both hemijoints of ACLF animals were similar to clinical findings in human PTOA and ACL injury patients. One study, for example, examined femoral and tibial bone changes at the hemijoint level in patients with mild radiographic knee OA and documented decreases in bone volume fraction in both hemijoints of the femur and tibia when compared with age matched control subjects[48]. Additionally, in both compartments of the osteoarthritic femurs and lateral tibia, trabecular number and trabecular bone thickness decreased while trabecular separation increased. A recent study investigating only the distal femur of subjects with mild radiographic knee OA found similar decreases in bone volume fraction in both the medial and lateral compartments compared to age-matched healthy control knees[49]. Although the cause of OA in these clinical studies is not precisely known, it appears that the dual-compartment changes in trabecular morphology and decreases in bone volume are similar to effects documented in the ACLF animals. It has also been shown clinically that following ACL injury, patients show decreased BMD in the tibia, femur and patella[50], a phenomenon that was also documented in the current study for the ACLF model. One limitation of the current study is the significant inter-species differences in cartilage and bone characteristics, which makes the direct comparison of these results to human studies challenging[51].

Decreases in bone volume and bone mineral density were identified in both the medial and lateral hemijoints of ACLF animals, while mACLT animals primarily had changes restricted to the medial hemijoint. ACLF animals also presented with more osteophytes and an increased extent of intermedullary edema. Overall, the findings of this study might suggest that the traumatically induced ACL and meniscal tear model better simulates clinical findings in the progression of a PTOA than does the mACLT model. This suggestion is largely supported by clinical data that identifies decreased quality and quantity of bone in OA patients, and identifies subchondral bone as an important target of OA intervention strategies. Additional studies, however, are still needed to further investigate changes in other joint tissues and to better track the chronic development of end-stage disease in this animal model.

Acknowledgments

Research reported in this publication was supported by the National Institute of Arthritis and Musculoskeletal and Skin Diseases of the National Institutes under award number R21 AR060464. The content is solely the responsibility of the authors and does not represent the official views of the National Institutes of Health. The

authors would like to acknowledge Ms. Jean Atkinson for the care of the animals of this study. The authors report no proprietary or commercial interest in any product mentioned or concept discussed in this article.

References

1. Gelber AC, Hochberg MC, Mead LA, et al. Joint injury in young adults and risk for subsequent knee and hip osteoarthritis. Ann Intern Med. 2000; 133(5):321–8. [PubMed: 10979876]
2. Felson DT. An update on the pathogenesis and epidemiology of osteoarthritis. Radiol Clin North Am. 2004; 42(1):1–9. [PubMed: 15049520]
3. Boden BP, Sheehan FT, Torg JS, Hewett TE. Noncontact anterior cruciate ligament injuries: mechanisms and risk factors. J Am Acad Orthop Surg. 2010; 18(9):520–7. [PubMed: 20810933]
4. Hewett TE, Stroupe aL, Nance Ta, Noyes FR. Plyometric Training in Female Athletes: Decreased Impact Forces and Increased Hamstring Torques. Am J Sports Med. 1996; 24(6):765–773. [PubMed: 8947398]
5. Faunø P, Wulff Jakobsen B. Mechanism of anterior cruciate ligament injuries in soccer. Int J Sports Med. 2006; 27(1):75–9. [PubMed: 16388446]
6. McGonagle D, Tan AL, Carey J, Benjamin M. The anatomical basis for a novel classification of osteoarthritis and allied disorders. J Anat. 2010; 216(3):279–91. [PubMed: 20070426]
7. Goldring SR. Role of Bone in Osteoarthritis Pathogenesis. Osteoarthritis. 2009; 93(1):25–35.
8. Teitelbaum SL. Osteoclasts: what do they do and how do they do it? Am J Pathol. 2007; 170(2): 427–35. [PubMed: 17255310]
9. Burr DB. The importance of subchondral bone in the progression of osteoarthritis. J Rheumatol Suppl. 2004; 70:77–80. [PubMed: 15132360]
10. Day JS, Ding M, van der Linden JC, et al. A decreased subchondral trabecular bone tissue elastic modulus is associated with pre-arthritic cartilage damage. J Orthop Res. 2001; 19(5):914–8. [PubMed: 11562141]
11. Li B, Aspden RM. Mechanical and material properties of the subchondral bone plate from the femoral head of patients with osteoarthritis or osteoporosis. Ann Rheum Dis. 1997; 56(4):247–54. [PubMed: 9165997]
12. Faibish D, Ott SM, Boskey AL. Mineral changes in osteoporosis: a review. Clin Orthop Relat Res. 2006; 443:28–38. [PubMed: 16462423]
13. Lane LB, Villacin A, Bullough PG. The vascularity and remodelling of subchondrial bone and calcified cartilage in adult human femoral and humeral heads. An age- and stress-related phenomenon. J Bone Joint Surg Br. 1977; 59(3):272–8. [PubMed: 893504]
14. Radin EL, Rose RM. Role of subchondral bone in the initiation and progression of cartilage damage. Clin Orthop Relat Res. 1986; (213):34–40. [PubMed: 3780104]
15. Burr DB, Schaffler MB. The involvement of subchondral mineralized tissues in osteoarthrosis: quantitative microscopic evidence. Microsc Res Tech. 1997; 37(4):343–57. [PubMed: 9185156]
16. Batiste DL, Kirkley A, Laverty S, et al. Ex vivo characterization of articular cartilage and bone lesions in a rabbit ACL transection model of osteoarthritis using MRI and micro-CT. Osteoarthritis Cartilage. 2004; 12(12):986–96. [PubMed: 15564066]
17. Bouchgua M, Alexander K, d'Anjou MA, et al. Use of routine clinical multimodality imaging in a rabbit model of osteoarthritis--part I. Osteoarthritis Cartilage. 2009; 17(2):188–96. [PubMed: 18760939]
18. Dedrick DK, Goldstein Sa, Brandt KD, et al. A longitudinal study of subchondral plate and trabecular bone in cruciate-deficient dogs with osteoarthritis followed up for 54 months. Arthritis Rheum. 1993; 36(10):1460–7. [PubMed: 8216405]
19. Boyd SK, Müller R, Leonard T, Herzog W. Long-term periarticular bone adaptation in a feline knee injury model for post-traumatic experimental osteoarthritis. Osteoarthritis Cartilage. 2005; 13(3):235–42. [PubMed: 15727890]
20. Hayami T, Pickarski M, Zhuo Y, et al. Characterization of articular cartilage and subchondral bone changes in the rat anterior cruciate ligament transection and meniscectomized models of osteoarthritis. Bone. 2006; 38(2):234–43. [PubMed: 16185945]

21. McDaniel WJ, Dameron TB. Untreated ruptures of the anterior cruciate ligament. A follow-up study. J Bone Joint Surg Am. 1980; 62(5):696–705. [PubMed: 7391092]
22. Atkinson PJ, Cooper TG, Anseth S, et al. Association of knee bone bruise frequency with time postinjury and type of soft tissue injury. Orthopedics. 2008; 31(5):440. [PubMed: 19292326]
23. Borrelli J, Zaegel Ma, Martinez MD, Silva MJ. Diminished cartilage creep properties and increased trabecular bone density following a single, sub-fracture impact of the rabbit femoral condyle. J Orthop Res. 2010; 28(10):1307–14. [PubMed: 20225288]
24. Newberry WN, Zukosky DK, Haut RC. Subfracture insult to a knee joint causes alterations in the bone and in the functional stiffness of overlying cartilage. J Orthop Res. 1997; 15(3):450–5. [PubMed: 9246093]
25. Ewers BJ, Weaver BT, Sevensma ET, Haut RC. Chronic changes in rabbit retro-patellar cartilage and subchondral bone after blunt impact loading of the patellofemoral joint. J Orthop Res. 2002; 20(3):545–50. [PubMed: 12038629]
26. Radin EL, Martin RB, Burr DB, et al. Effects of mechanical loading on the tissues of the rabbit knee. J Orthop Res. 1984; 2(3):221–34. [PubMed: 6436458]
27. Fischenich KM, Coatney Ga, Haverkamp JH, et al. Evaluation of meniscal mechanics and proteoglycan content in a modified anterior cruciate ligament transection model. J Biomech Eng. 2014; 136(7):1–8.
28. Intema F, Hazewinkel HaW, Gouwens D, et al. In early OA, thinning of the subchondral plate is directly related to cartilage damage: results from a canine ACLT-meniscectomy model. Osteoarthritis Cartilage. 2010; 18(5):691–8. [PubMed: 20175978]
29. Bellabarba C, Bush-Joseph CA, Bach BR. Patterns of meniscal injury in the anterior cruciate-deficient knee: a review of the literature. Am J Orthop (Belle Mead NJ). 1997; 26(1):18–23. [PubMed: 9021030]
30. Isaac DI, Meyer EG, Haut RC. Development of a traumatic anterior cruciate ligament and meniscal rupture model with a pilot in vivo study. J Biomech Eng. 2010; 132(6):064501–4. [PubMed: 20887035]
31. Isaac DI, Meyer EG, Haut RC. Chondrocyte damage and contact pressures following impact on the rabbit tibiofemoral joint. J Biomech Eng. 2008; 130(4):041018. [PubMed: 18601460]
32. Fischenich KM, Button KD, Coatney Ga, et al. Chronic Changes in the articular cartilage and meniscus following traumatic impact to the lapine knee. J Biomech. 2014; 2(21):246–253. [PubMed: 25523754]
33. Batiste DL, Kirkley A, Laverty S, et al. High-resolution MRI and micro-CT in an ex vivo rabbit anterior cruciate ligament transection model of osteoarthritis. Osteoarthritis Cartilage. 2004; 12(8): 614–26. [PubMed: 15262241]
34. Thompson WO, Fu FH. The meniscus in the cruciate-deficient knee. Clin Sports Med. 1993; 12(4): 771–96. [PubMed: 8261525]
35. Warren RF, Levy IM. Meniscal lesions associated with anterior cruciate ligament injury. Clin Orthop Relat Res. 1983; (172):32–7. [PubMed: 6822002]
36. Shoemaker SC, Markolf KL. The role of the meniscus in the anterior-posterior stability of the loaded anterior cruciate-deficient knee. Effects of partial versus total excision. J Bone Joint Surg Am. 1986; 68(1):71–9. [PubMed: 3753605]
37. Sharma L, Eckstein F, Song J, et al. Relationship of meniscal damage, meniscal extrusion, malalignment, and joint laxity to subsequent cartilage loss in osteoarthritic knees. Arthritis Rheum. 2008; 58(6):1716–26. [PubMed: 18512777]
38. Boyd SK, Matyas JR, Wohl GR, et al. Early regional adaptation of periarticular bone mineral density after anterior cruciate ligament injury. J Appl Physiol. 2000; 89(6):2359–64. [PubMed: 11090590]
39. Bouchgua M, Alexander K, Carmel EN, et al. Use of routine clinical multimodality imaging in a rabbit model of osteoarthritis--part II: bone mineral density assessment. Osteoarthritis Cartilage. 2009; 17(2):197–204. [PubMed: 18757215]
40. Messner K, Fahlgren a, Ross I, Andersson B. Simultaneous changes in bone mineral density and articular cartilage in a rabbit meniscectomy model of knee osteoarthrosis. Osteoarthritis Cartilage. 2000; 8(3):197–206. [PubMed: 10806047]

41. McErlain DD, Appleton CTG, Litchfield RB, et al. Study of subchondral bone adaptations in a rodent surgical model of OA using in vivo micro-computed tomography. Osteoarthritis Cartilage. 2008; 16(4):458–69. [PubMed: 17900933]
42. Cake, Ma; Read, Ra; Appleyard, RC., et al. The nitric oxide donor glyceryl trinitrate increases subchondral bone sclerosis and cartilage degeneration following ovine meniscectomy. Osteoarthritis Cartilage. 2004; 12(12):974–81. [PubMed: 15564064]
43. Isaac DI, Meyer EG, Kopke KS, Haut RC. Chronic changes in the rabbit tibial plateau following blunt trauma to the tibiofemoral joint. J Biomech. 2010; 43(9):1682–8. [PubMed: 20399435]
44. Brandt KD. Osteophytes in osteoarthritis. Clinical aspects. Osteoarthritis Cartilage. 1999; 7(3): 334–5. [PubMed: 10329321]
45. Nakamae A, Engebretsen L, Bahr R, et al. Natural history of bone bruises after acute knee injury: clinical outcome and histopathological findings. Knee Surg Sports Traumatol Arthrosc. 2006; 14(12):1252–8. [PubMed: 16786336]
46. Hernández-Molina G, Guermazi A, Niu J, et al. Central bone marrow lesions in symptomatic knee osteoarthritis and their relationship to anterior cruciate ligament tears and cartilage loss. Arthritis Rheum. 2008; 58(1):130–6. [PubMed: 18163483]
47. Lo GH, Hunter DJ, Zhang Y, et al. Bone marrow lesions in the knee are associated with increased local bone density. Arthritis Rheum. 2005; 52(9):2814–21.145676. [PubMed: 16145676]
48. Bolbos RI, Zuo J, Banerjee S, et al. Relationship between trabecular bone structure and articular cartilage morphology and relaxation times in early OA of the knee joint using parallel MRI at 3 T. Osteoarthritis Cartilage. 2008; 16(10):1150–9. [PubMed: 18387828]
49. Chang G, Xia D, Chen C, et al. 7T MRI detects deterioration in subchondral bone microarchitecture in subjects with mild knee osteoarthritis as compared with healthy controls. J Magn Reson Imaging. 2014; 00:1–7.
50. Leppälä J, Kannus P, Natri A, et al. Effect of anterior cruciate ligament injury of the knee on bone mineral density of the spine and affected lower extremity: a prospective one-year follow-Up study. Calcif Tissue Int. 1999; 64(4):357–63. [PubMed: 10089231]
51. Chevrier A, Kouao ASM, Picard G, et al. Interspecies comparison of subchondral bone properties important for cartilage repair. J Orthop Res. 2015; 33(1):63–70. [PubMed: 25242685]

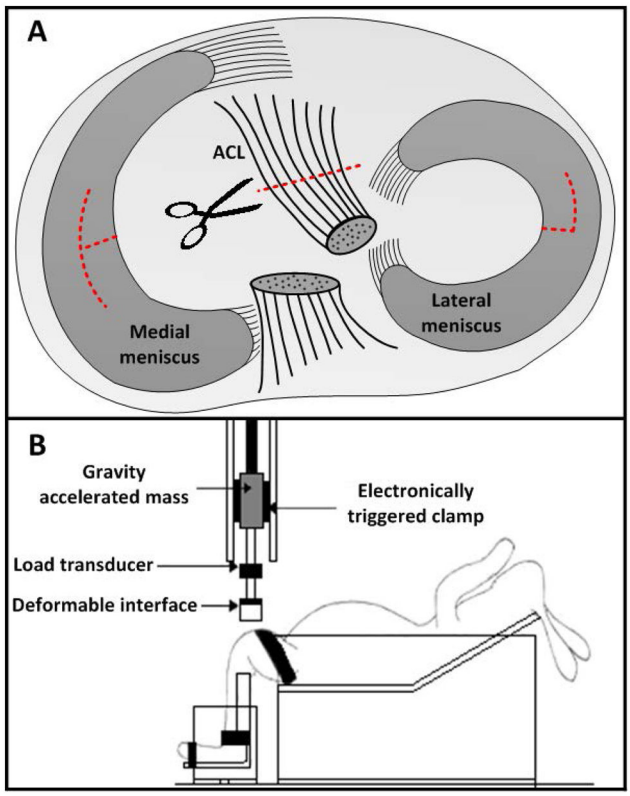

Figure 1.
(A) Diagram of meniscal and ACL transections in the mACLT model. (B) Diagram of the traumatic impact setup used for the ACLF model.

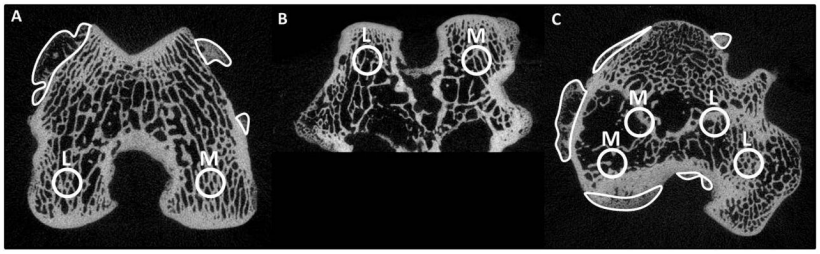

Figure 2.

μCT images of (A) a femur transverse cut, (B) a femur axial cut, and (C) a tibia transverse cut for rabbits 12 weeks post-injury that show manual outlines of osteophytes (A and C) and placement of VOIs (volume of interest). M=medial VOIs and L=lateral VOIs.

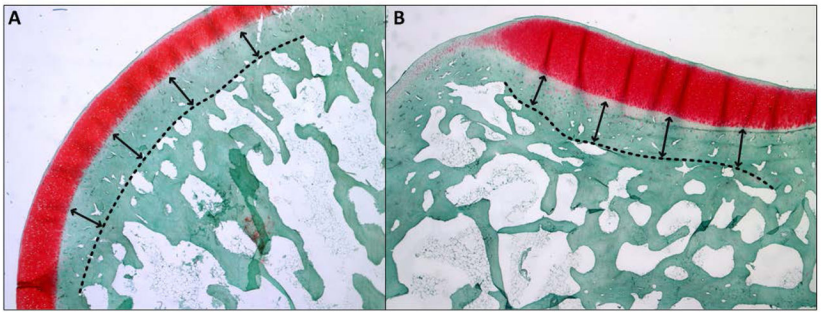

Figure 3.

Histology images of a representative (A) femoral condyle and (B) tibial plateau showing the method for determining subchondral bone thickness using Hematoxlyin, Safranin-O, and Fast Green staining techniques.

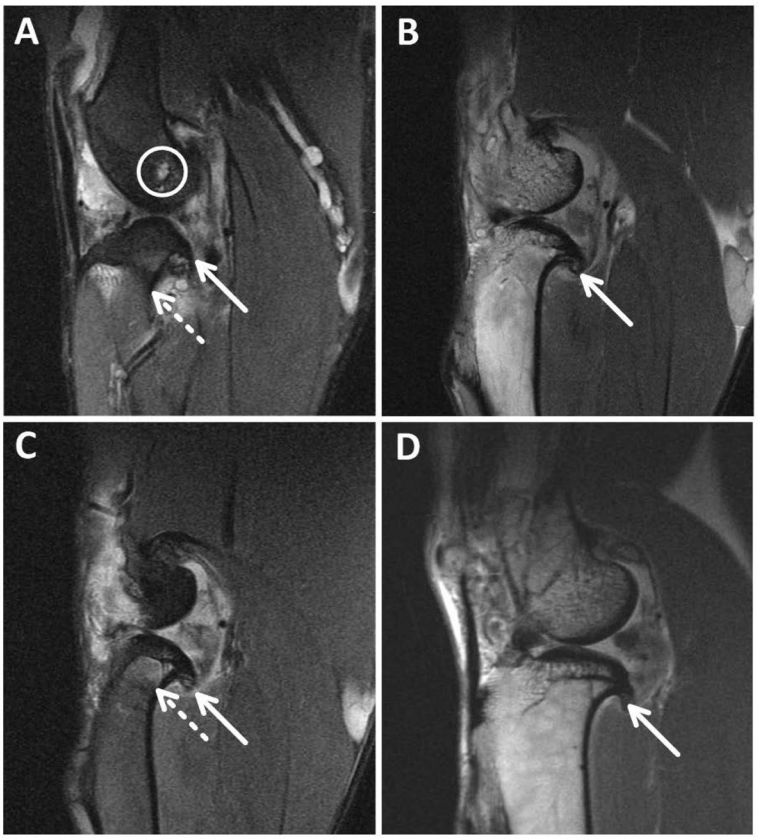

Figure 4.

Representative MRI's for A) ACLF animal with a white circle outlining the ganglion cyst. B) and C) are from an ACLF animal showing osteophytes and edemas, d) mACLT animal showing osteophytes. Solid arrows identify osteophytes where as dashed arrows identify edemas.

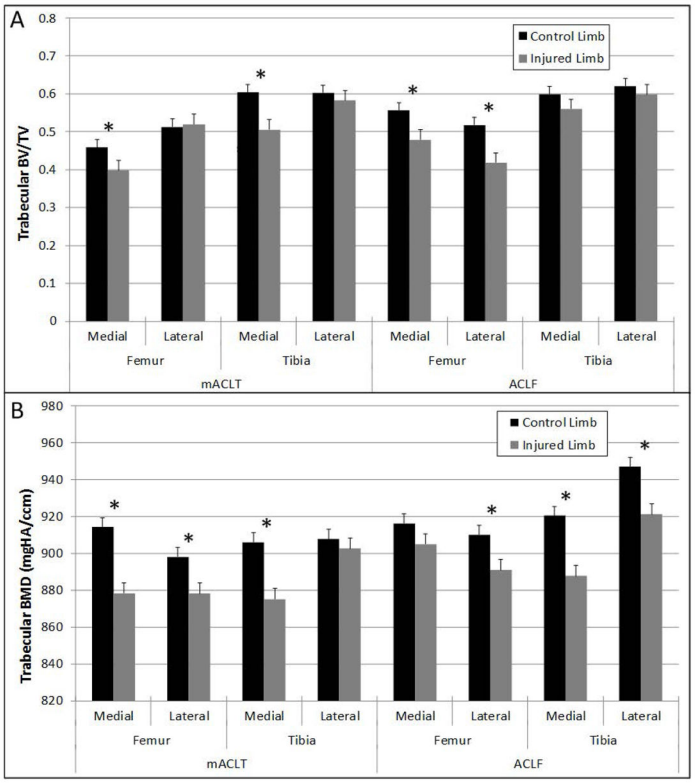

Figure 5.

(A) Trabecular bone volume fraction values and (B) trabecular bone mineral density values of control and injured mACLT and ACLF femurs and tibias. * denotes statistical differences between control and injured limbs at $p<0.05$. Data shown is mean ± standard error.

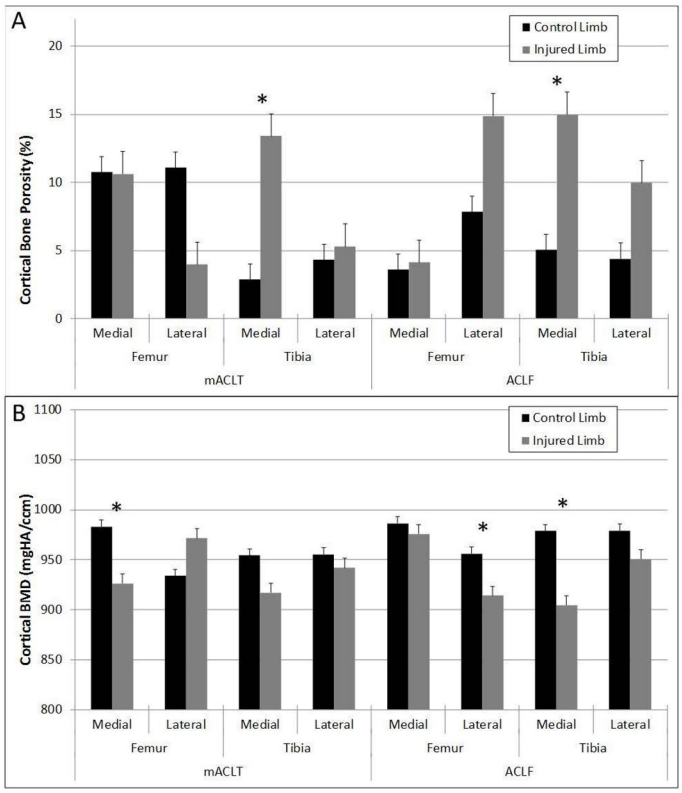

Figure 6.

(A) Cortical bone porosity values and (B) cortical bone mineral density values of control and injured mACLT and ACLF femurs and tibias. * denotes statistical differences between control and injured limbs at $p<0.05$. Data shown is mean ± standard error.

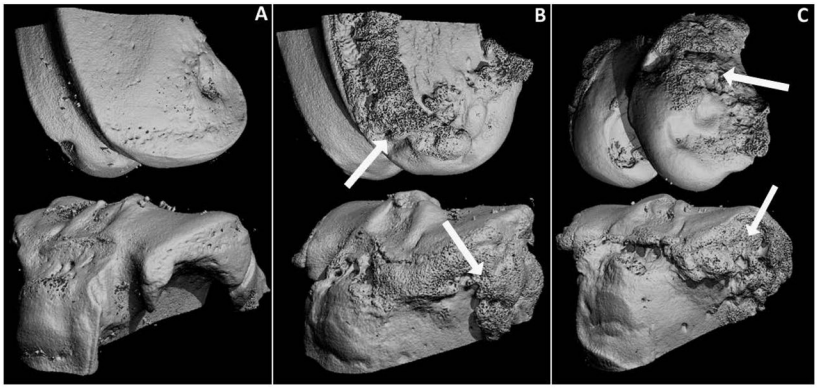

Figure 7.

3-Dimensional reconstructions of a representative (A) control knee, (B) an mACLT injured knee and (C) an ACLF injured knee 12 weeks post-injury. Prominent osteophytes were evident on the injured femurs and tibias (arrows).

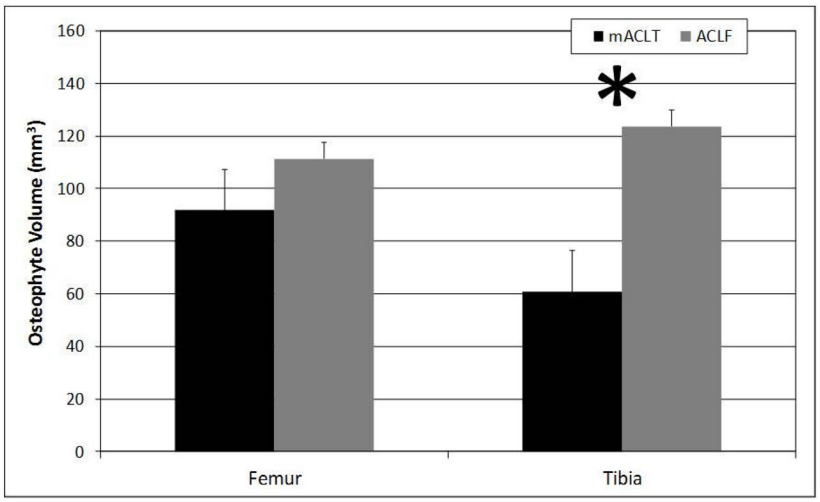

Figure 8.

Volume of osteophytes (mm^3) on injured femurs and tibias of mACLT and ACLF animals. * denotes statistical differences between mACLT and ACLF animals at $p<0.05$. Data shown is mean ± standard error.

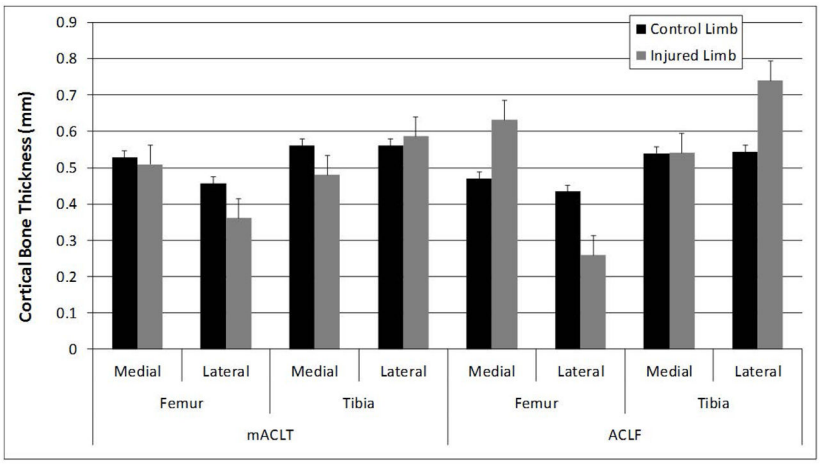

Figure 9.

Cortical bone thickness of control and injured mACLT and ACLF femurs and tibias. * denotes statistical differences between control and injured limbs at $p<0.05$. Data shown is mean ± standard error.

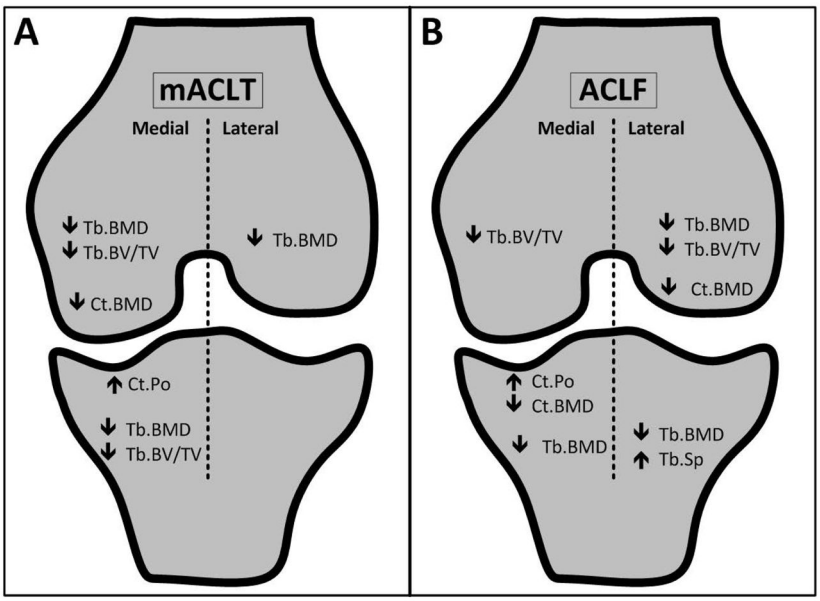

Figure 10.
Schematic showing significant hemijoint level changes in the femurs and tibias of mACLT and ACLF animals.

Table 1

Trabecular bone metrics in control and injured limbs for mACLT and ACLF femurs and tibias (mean ± standard error).

				Trabecular Number (mm^{-1})	Trabecular Thickness (mm)	Trabecular separation (mm)
mCLTA	Femur	Control	Medial	2.32 ± 0.30	0.20 ± 0.02	0.24 ± 0.06
			Lateral	2.55 ± 0.10	0.22 ± 0.02	0.19 ± 0.03
		Injured	Medial	2.36 ± 0.10	0.17 ± 0.01	0.25 ± 0.03
			Lateral	2.55 ± 0.12	0.21 ± 0.02	0.19 ± 0.03
	Tibia	Control	Medial	2.54 ± 0.21	0.25 ± 0.03	0.15 ± 0.02
			Lateral	2.49 ± 0.26	0.26 ± 0.03	0.15 ± 0.03
		Injured	Medial	2.72 ± 0.29	0.19 ± 0.02	0.19 ±0.04
			Lateral	2.51 ± 0.25	0.25 ± 0.02	0.16 ± 0.03
ACLF	Femur	Control	Medial	2.43 ± 0.08	0.24 ± 0.01	0.18 ± 0.02
			Lateral	2.44 ± 0.16	0.22 ± 0.01	0.19 ± 0.02
		Injured	Medial	2.34 ± 0.12	0.21 ± 0.02	0.22 ± 0.02
			Lateral	2.29 ± 0.21	0.19 ± 0.03	0.26 ± 0.03
	Tibia	Control	Medial	2.43 ± 0.28	0.25 ± 0.03	0.17 ± 0.07
			Lateral	2.35 ± 0.15	0.27 ± 0.32	**0.15 ± 0.02***
		Injured	Medial	2.60 ± 0.20	0.23 ± 0.02	0.16 ± 0.03
			Lateral	2.30 ± 0.35	0.27 ± 0.05	0.21 ± 0.19

*denotes a statistical difference between control and affected limbs at $p<0.05$.